

Guided filter-based images fusion algorithm for CT and MRI medical images

ISSN 1751-9659

Received on 27th November 2016

Revised 29th July 2017

Accepted on 8th October 2017

E-First on 22nd November 2017

doi: 10.1049/iet-ipr.2016.0920

www.ietdl.org

Yan Na¹ , Li Zhao¹, Yingxue Yang², Mengqiao Ren¹

¹School of Electronic Engineering, Xidian University, Xi'an, Shaanxi, People's Republic of China

²Hospital of Xidian University, Xi'an, Shaanxi, People's Republic of China

 E-mail: yna@mail.xidian.edu.cn

Abstract: A novel fusion algorithm based on guided filter (GF) for computed tomography (CT) and magnetic resonance imaging (MRI) medical images is proposed. In this algorithm: approximation coefficient and three wavelet coefficients of CT and MRI are obtained by the wavelet transform, respectively. Two weight maps are obtained by comparison of the pixel values of the two approximation coefficients. A GF is designed with the weight maps serving as the input image and the corresponding approximation coefficient serving as the guided image; the GF is used to smooth the weight images and refined weight maps are obtained. The approximation and wavelet coefficients of CT and MRI images are fused by the weighted fusion algorithm with refined weight maps. A fused image of CT and MRI is obtained by the inverse wavelet transform. Comparisons of this algorithm with two fusion algorithms available show that the fused image based on this algorithm contains a greater amount of information, more details and clearer edges than the other two algorithms. Therefore, this algorithm is better at locating the position and shape of the target volume. In the course of treatment, this algorithm can better avoid the surrounding health organs by radiation, protect the health of patients.

1 Introduction

Medical images obtained by different imaging technologies provide different information for clinical diagnosis. Computed tomography (CT) and magnetic resonance imaging (MRI) images both can be used in medical diagnosis [1].

CT is to use computer controlled X-ray to scan human body section and generate density difference images due to different human tissues have different densities and radial absorption rate. CT has high-density resolution for density difference tissues but low resolution for soft tissues.

Chest CT is crucial for early lung cancer diagnosis, high-resolution CT scanner further improves the resolution of lung diagnosis. This is significant for some diseases such as interstitial lung disease.

In tumour treatment, doctor's clinical experience and different understandings of anatomical structure and target volume confirmation using CT scanner will make differences in describing the boundary of tumour target region and outline of normal tissues [2].

MRI is a biology nuclear magnetic spin imaging technology. MRI has unique advantages in imaging of nervous system, articular cartilage, muscle, fat and soft tissue lesions, but cannot be used for imaging of density bone, calcification and gas lung. So, on MRI image, soft tissue is clear [3].

MRI has advantage in soft tissue imaging, where CT can be used for bone tissue and lung. MRI is more versatile than CT especially for brain, spine and myelopathy [4], it is also a reliable diagnosis technique for heart disease and cardiac function test due to its capability of showing the tiny cardiac element.

CT and MRI are the most common imaging methods for clinical disease diagnosis, the new patient image acquired by fusing the CT and MRI images will combine the advantages of two imaging techniques and make up the deficiency of single imaging pattern, the fusion image will contain more abundant, visual and comprehensive information, acquiring new diagnosis information by fusion imaging will be helpful for precisely identifying spatial location, size, geometrical shape of lesion [5] and increasing the accuracy of disease diagnosis.

Radiation oncology is transforming from general external irradiation to precision radiotherapy such as stereotactic radiotherapy, three-dimensional conformal radiotherapy and intensity modulated radiation therapy, the definition accuracy between gross tumour volume and normal tissue is the assessment criteria for tumour radiotherapy treatment plan [6]. Experienced radiotherapist can evaluate the CT target volume, MRI target volume and CT and MRI fusion target volume to acquire higher accuracy clinical diagnosis for the tumour target volume and will benefit for patient precision targeted therapy [7].

There is evidence showed that malignant tumour postoperative target identified by radiotherapist utilising CT and MRI fusion imaging will be smaller than CT positioning imaging, CT and MRI fusion will reduce the volume normal tissue exposed to radiation source and improve the target volume dosage, narrow the diagnosis discrepancies between different physicians and better protect the patients [8].

At present, common medical images fusion algorithms are implemented at different scales, different resolutions and different decomposition levels [9]. First, multi-resolution decomposition is adopted on source images. Then, the decomposed coefficients are fused to get a fused image. Currently, there are many fusion algorithms. Choose-max fusion algorithm [10] is a simple implementation, but it is noise sensitive. Weighted average fusion algorithm has a wide range of applications, but it reduces the image contrast and loses the edge information, and its anti-interference ability is poor which reduces the SNR of the image [11]. Intuitionistic fuzzy inference-based fusion algorithms are easy to produce the 'either/or' result and cause misjudgement because there is no criterion for the division of pixels and domain of discourse, and it is difficult to choose a subordinating degree function [12]. Generally speaking, in fusion algorithms available, fixed weighted coefficients are adopted. So, these fusion algorithms lack adaptability.

In the field of image processing, we often need to use a variety of filters, we use these filters for image enhancement, smoothing, edge extraction and other operations. These image processing filters can be divided into linear shift invariant filter and shift variant filter. Linear shift invariant filter kernel weights are unchanged, for all of the image content is the same operation, and

the input image content information is not related, such as median filter. The kernel weight of the shift variant filter is not fixed, which is related to the content information of the image, such as bilateral filter, cross bilateral filter. We call this kind of image as the guided image, and filter which is determined by the content of image is named as guided filter (GF). Input image or another image can be used as guided image. The advantage of the GF is that the output image can not only keep the image content information of the source image but also get the characteristic of the guided image.

Bilateral filter is a kind of GF which is constructed on the basis of Gauss filter [13]. The kernel of bilateral filter should not only consider the spatial distance between image pixels but also include the difference information of the pixels in the input image. Therefore, it does not cause image blurring when smoothing image, it can filter the noise while preserving the edges. Based on this excellent property, bilateral filter is applied to many aspects of image processing. However, the guided image of the bilateral filter is its input image, and most of the time we want to get some information out of the input image. This requires the use of another image in the design of the filter kernel, so that it plays a guided role in the image information. There is a joint bilateral filter [14], its input and guided images are different images, and the kernel weight of filter is determined by the content information of the additional guided image. However, there are some shortcomings in the bilateral filter and the joint bilateral filter, for example, in the application of the detail enhancement, there is obvious edge gradient inversion [15].

The latest image GF was proposed in [16]. The GF also has the characteristics of keeping the edge of the image while removing the image noise. The guide filter overcomes the defects such as the edge gradient inversion in the bilateral filter. One of the more obvious advantages of the algorithm is that the complexity of the algorithm is linear. The size of the window is not related, the efficiency is very high.

A novel CT and MRI medical images weighted fusion algorithm based on GF is proposed in this paper in order to fuse images adaptively. In this algorithm, approximation coefficient and three wavelet coefficients of CT and MRI are obtained by using a wavelet transform on CT and MRI medical images, respectively. Due to the two approximation coefficients maintaining the overall shape of the source images, they are compared pixel by pixel to determine the weight maps. The weight maps obtained are usually noisy and have edge blurring. By using the weight maps to obtain a fused image usually produces artefacts. So, in this paper, a GF is designed with the weight maps serving as the input image and the corresponding approximation coefficient serving as the guided image, the GF is used to smooth the weight images and refined weight maps are obtained. Thus, the refined weight map of each image is different and determined by the characteristics of the image to be fused. The approximation and wavelet coefficients of CT and MRI images are fused together by the weighted fusion algorithm using the refined weight maps. A fused image of CT and MRI is obtained by the inverse wavelet transform.

Comparisons of this algorithm with Choose-max fusion algorithm and Intuitionistic fuzzy inference fusion algorithm show that the fused image based on this algorithm contains a greater amount of information, more details and clearer edges. The fused image is obviously better on both subjective and objective evaluations. Medical evaluations show that this algorithm is more advantageous than the other two algorithms to locate the position and shape of the target volume, and improve the target volume delineation efficiency. In the course of treatment, this method can better avoid the surrounding health organs by radiation, protect the health of patients.

This paper is organised as follows: ‘the method is introduced in Section 2, main content is introduction to the GF and determination of parameters of the GF. CT and MRI images fusion based on GF is discussed in Section 3. Experimental results and discussion are in Section 4. Finally, a conclusion is presented in Section 5.

2 Method

The kernels of linear translation-invariant filters like the Gaussian filter are spatially invariant and independent of any image content. However, in many cases, we may want to incorporate additional information from a given guided image during the filtering process. That is to say, the kernel of the filter is determined by a guided image. The concept of the GF is put forward in [16]. The guided image can be the input image of the filter or another image. The GF has the ability of smoothing the image while preserving the edges [16]. The GF performs very well on many applications such as image enhancement [17], noise reduction [18], image dehazing [19] and images fusion [20].

2.1 Introduction to the GF

A filter output image O is a linear transformation of a guided image I [16]. In a window, ω_k centred at pixel k , the filter output O_i at pixel i is obtained as follows:

$$O_i = a_k I_i + b_k, \quad \forall i \in \omega_k \quad (1)$$

where ω_k is a square window of radius r . From (1), we can know that $\nabla O = a \nabla I$, where ∇O and ∇I are the gradients of output image O and guided image I . It means O has an edge only if I has an edge. a_k and b_k are linear coefficients in ω_k and can be estimated by minimising the following cost function in the local window:

$$E(a_k, b_k) = \sum_{i \in \omega_k} ((a_k I_i + b_k - P_i)^2 + \epsilon a_k^2) \quad (2)$$

where ϵ is an important parameter to adjust the filtering effect that will be discussed later in detail; P_i is the value of input image P at pixel i . a_k and b_k can be solved by the least-square method as follows:

$$a_k = \frac{1/|\omega| \sum_{i \in \omega_k} I_i P_i - \mu_k \bar{P}_k}{\sigma_k^2 + \epsilon} \quad (3)$$

$$b_k = \bar{P}_k - a_k \mu_k$$

where μ_k and σ_k^2 are the mean and deviation value of the guided image in ω_k . $|\omega|$ represents the pixel numbers in ω_k . \bar{P}_k is the mean value of the input image in ω_k . When calculating the linear coefficients of each window, we can find that a pixel can be included in multiple Windows. That is to say, each pixel is described by multiple linear functions and the value of O_i is diverse when it is computed in different windows. To solve this problem, all possible values of O_i need to be averaged first

$$O_i = \frac{1}{|\omega|} \sum_{i \in \omega_k} (a_k I_i + b_k) \quad (4)$$

$$= \bar{a}_i I_i + \bar{b}_i$$

where $\bar{a}_i = (1/|\omega|) \sum_{k \in \omega_i} a_k$, $\bar{b}_i = (1/|\omega|) \sum_{k \in \omega_i} b_k$. Now ∇O is no longer the linear transformation of ∇I , because the linear coefficients \bar{a}_i and \bar{b}_i vary spatially. However, since the coefficients are the output of an average filter, their gradients should be much smaller than that of I near the strong edges. So we still have $\nabla O \approx a \nabla I$. That means obvious edges in I can be mostly maintained in O , which demonstrates the edge preserving feature of the GF.

2.2 Determination of parameters of the GF

$G_{r,\epsilon}(P, I)$ is used to represent the GF in this paper. P and I refer to the input image and guided image, respectively. r and ϵ are parameters that determine the filter size and blur the degree of the GF, respectively.

In the condition that $I = P$, the GF serves as an edge preserving filter. At present, $a_k = \sigma_k^2 / (\sigma_k^2 + \epsilon)$, $b_k = (1 - a_k) \mu_k$. If $\epsilon = 0$, it is

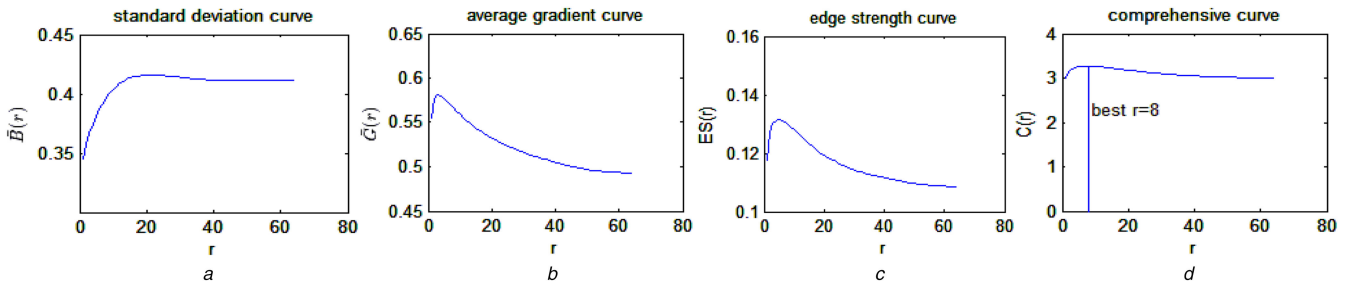


Fig. 1 Relationship curve between r and evaluation parameters of group one of testing images

(a) Relationship curve between r and $\bar{B}(r)$, (b) Relationship curve between r and $\bar{G}(r)$, (c) Relationship curve between r and $ES(r)$, (d) Relationship curve between r and $C(r)$

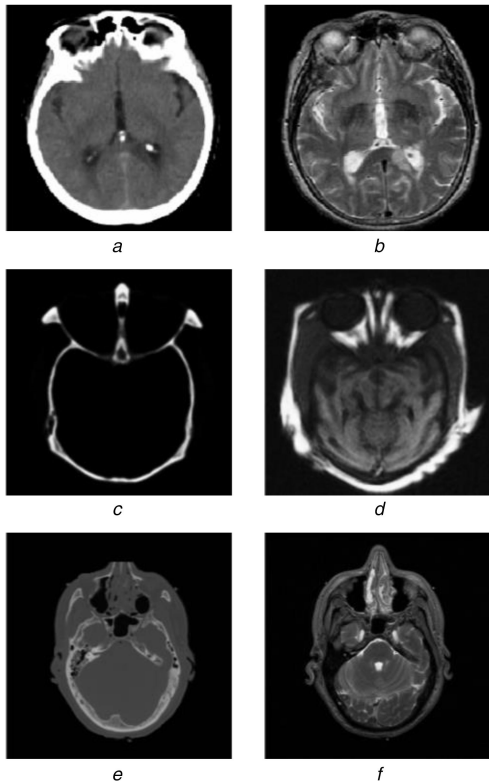


Fig. 2 Testing images of group one, group two and group three

(a) CT image of group one, (b) MRI image of group one, (c) CT image of group two, (d) MRI image of group two, (e) CT image of group three, (f) MRI image of group three

obvious that $a_k = 1$, $b_k = 0$. From (1), we know that the output $O = I$, so no filtering effect is present at this time.

If $\epsilon > 0$, let us consider two cases:

Case 1: 'High variance'. If guided image I changes a lot in ω_k , we have $\sigma_k^2 \gg \epsilon$, so $a_k \approx 1$ and $b_k \approx 0$. Then, the spatial filtering effect is very weak and the filter can help to maintain the edges of the image.

Case 2: 'Flat patch'. If guided image I is almost constant in ω_k , we have $\sigma_k^2 \ll \epsilon$, so $a_k \approx 0$ and $b_k \approx \mu_k$. Then, it serves as a weighted average filter.

The parameter ϵ is the criterion to determine a 'high variance' or a 'flat patch'. The patches with a variance much smaller than ϵ are smoothed, while those with a variance much larger than ϵ are preserved. Under the condition that the window size is unchangeable, the smaller the ϵ , the more obvious that the features of edge preservation. The larger the ϵ , the more obvious the filtering effect.

In fusion of CT and MRI images, more details and edge information are expected to be included in fused image. According to the above discussion, these features should correspond to 'high variance' zone. So, variance is much larger than ϵ .

This paper adopts the following method to determine the value of ϵ .

First, let r be 3. (r can take any value in the range of r , because ϵ has nothing to do with the value of r and ϵ is related to the relative size of variance.)

Second, calculate evaluation parameters when the value of ϵ is changed from $\sigma^2 \times 10^{-10}$ to $\sigma^2 \times 10^{-25}$, the change method of ϵ is that the value of ϵ in next step is the multiplication of previous one by 10^{-1} . Where σ^2 is deviation value of the guided image.

After analysing evaluation parameters, we find that all the evaluation parameters will remain at a fixed value with a very little variation when value of ϵ is a relatively very small one to σ^2 .

By comparing these evaluation parameters, we also find the value of ϵ should be less than $\sigma^2 \times 10^{-15}$.

So $\epsilon = \sigma^2 \times 10^{-20}$ is taken in this paper.

The relationship curve of r corresponding to evaluation parameters can be obtained by traversing r , and then the best value of r can be determined with this curve.

From the theoretical knowledge of GF, the minimum value of r is 1 and the maximum value of r is $(\min(\text{width} - 1, \text{height} - 1))/2$, where width is the pixel number of guided image in the x direction and height is the pixel number of guided image in the y direction, min is the minimum operation.

In this paper, the method to determine the value of r is as follows.

First, evaluation parameters are recorded as $\bar{B}(1)$, $\bar{G}(1)$, $ES(1)$ when $r=1$.

Second, comprehensive evaluation parameters are recorded as $C(r) = \bar{B}(r)/\bar{B}(1) + \bar{G}(r)/\bar{G}(1) + ES(r)/ES(1)$ when traversing r with step of 1.

Finally, the maximum value of $C(r)$ corresponds to the best r .

$\bar{B}(r)$ represents standard deviation about r , $\bar{B}(1)$ represents standard deviation when $r=1$, $\bar{G}(r)$ represents average gradient about r , $\bar{G}(1)$ represents average gradient when $r=1$, $ES(r)$ represents edge strength about r , $ES(1)$ represents edge strength when $r=1$.

The definition of \bar{B} , \bar{G} and ES is in Section 3.3.

An example of the relationship curve between r and evaluation parameters is shown in Fig. 1.

In Fig. 1, the relationship curve is obtained with the group one of testing images (in Fig. 2) and the best r is 8. Different groups have different relationship curve and have different best r . The experimental results of the proposed algorithm are obtained at the best r of every group itself.

3 CT and MRI images fusion based on GF

3.1 Scheme of CT and MRI images fusion based on GF

Fig. 3 shows the scheme of CT and MRI images fusion based on GF.

First, wavelet transform [21] is applied to each source images after registration. A CT image is decomposed into approximation coefficient A_1 and three wavelet coefficients H_1 , V_1 , D_1 . An MRI image is decomposed into approximation coefficient A_2 and three

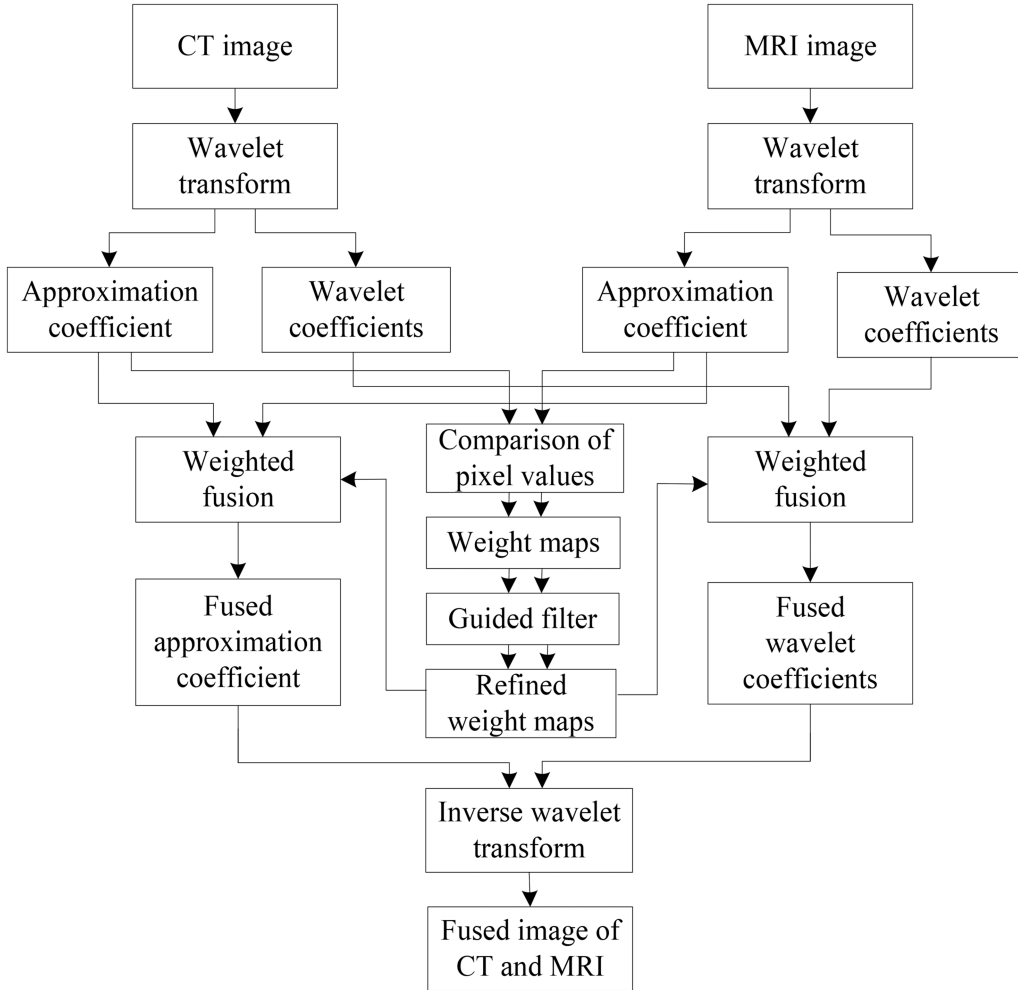


Fig. 3 Scheme of CT and MRI images fusion based on GF

wavelet coefficients H_2 , V_2 , D_2 . The wavelet transform aims at separating each source image into a low-frequency coefficient containing large-scale approximate information and three high-frequency coefficients containing small-scale detail information.

Second, because two approximation coefficients A_1 and A_2 maintain the overall shape of the source images, the weight maps W_1 and W_2 are obtained by comparison of the pixel values of the two approximation coefficients:

$$W_1 = \begin{cases} 1 & \text{if } A_1 > A_2 \\ 0 & \text{otherwise} \end{cases} \quad (5)$$

$$W_2 = \begin{cases} 1 & \text{if } A_2 > A_1 \\ 0 & \text{otherwise} \end{cases}$$

The weight maps obtained by (5) are usually noisy and have edge blurring. Using the weight maps to obtain a fused image directly will produce artefacts. In order to determine the position more accurately, we need to provide a fused image with more clear edges. A GF is designed with the weight maps W_1 and W_2 serving as the input image, respectively, and the corresponding approximation coefficient A_1 and A_2 serving as the guided image, respectively; then, the GF is used to smooth weight maps. The values of r and ϵ are automatically obtained by the method in Section 2.2, and different group of images may have different values. Then, the refined weight maps M_1 and M_2 are obtained

$$M_1 = G_{r,\epsilon}(W_1, A_1) \quad (6)$$

$$M_2 = G_{r,\epsilon}(W_2, A_2)$$

Third, the two approximation coefficients A_1 and A_2 are fused to obtain the fused approximation coefficient A by the weighted

fusion algorithm using refined weight maps. The three wavelet coefficients H_1 and H_2 , V_1 and V_2 , and D_1 and D_2 are fused, respectively, to obtain the fused wavelet coefficients H , V , D by using the weighted fusion algorithm

$$\begin{aligned} A &= A_1 \times M_1 + A_2 \times M_2 \\ H &= H_1 \times M_1 + H_2 \times M_2 \\ V &= V_1 \times M_1 + V_2 \times M_2 \\ D &= D_1 \times M_1 + D_2 \times M_2 \end{aligned} \quad (7)$$

Finally, the fused approximation and wavelet coefficients A , H , V , D are operated by inverse wavelet transform to obtain a fused image.

3.2 Testing images used in the experiment

Experiments are performed on 15 groups of testing images as shown in Figs. 2, 4–7. Each pair of CT and MRI images is the same body parts of the same person after registration.

3.3 Evaluation parameters

In order to assess the fusion performance of different algorithms objectively, the fused images are also analysed in terms of three objective evaluations: ‘standard deviation, average gradient and edge strength. Suppose that the testing image B is of size $M \times N$, where M and N are the rows and columns of the image, respectively. B means fused images and $B_{i,j}$ means the value at pixel (i, j) .

The mean value of fused image \bar{B} is defined as follows:

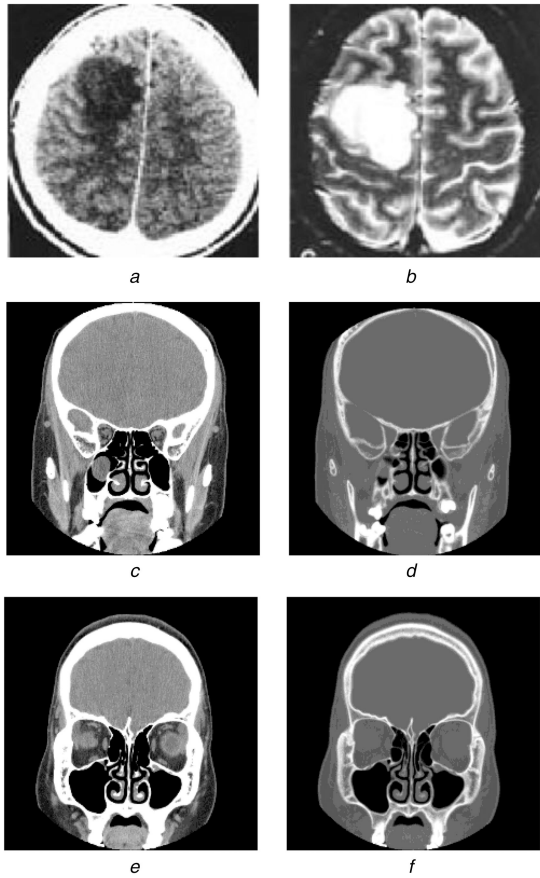


Fig. 4 Testing images of group four, group five and group six
 (a) CT image of group four, (b) MRI image of group four, (c) CT image of group five,
 (d) MRI image of group five, (e) CT image of group six, (f) MRI image of group six

$$\bar{B} = \frac{\sum_{i=1}^M \sum_{j=1}^N B_{i,j}}{M \times N} \quad (8)$$

The average gradient \bar{G} reflects the marginalisation degree and the tiny detail contrast of an image. The larger the average gradient of an image, the higher the image clarity [22]. A Sobel operator is used to calculate the first-order partial derivative of image B . The average gradient \bar{G} is defined as follows:

$$\bar{G} = \frac{1}{(M-1) \times (N-1)} \sum_{i=1}^{M-1} \sum_{j=1}^{N-1} \sqrt{\frac{(S_x(i,j)^2 + S_y(i,j)^2)}{2}} \quad (9)$$

where $S_x(i,j)$, $S_y(i,j)$ represent the first-order partial derivative in horizontal and vertical directions at point (i,j) : (see (10))

The edge strength reflects the image clarity degree. The more abundant the image detail and edge, the higher the image clarity [23]. A method proposed by Wu Lin is used to calculate the edge strength [24]. Neighbourhood pixel values are used to calculate the second-order partial derivative in four directions (horizontal, vertical, diagonal and back-diagonal), which are expressed as $HOE(i,j)$, $VOE(i,j)$, $DOE(i,j)$ and $BOE(i,j)$, respectively, in formula (11) (see (11))

Then, the maximum value in the four directions is selected as the edge strength at pixel (i,j) . The edge strength ES of image B is obtained by averaging all of the edge strengths of each pixel

$$ES = \frac{1}{M \times N} \sum_{i=1}^M \sum_{j=1}^N \max \left\{ HOE(i,j), VOE(i,j), DOE(i,j), BOE(i,j) \right\} \quad (12)$$

3.4 Comparison algorithm

Fusion algorithm proposed in this paper is compared with the following two fusion algorithms.

3.4.1 Choose-max fusion algorithm: The choose-max fusion algorithm is to compare the gray value of each pixel in the input image, and take the larger gray value as the gray value of the fused image.

The step of choose-max fusion algorithm is as follows:

Step one: ‘wavelet transform is applied to each source image after registration. CT image is decomposed into approximation coefficient A_1 and three wavelet coefficients H_1 , V_1 , D_1 . MRI image is decomposed into approximation coefficient A_2 and three wavelet coefficients H_2 , V_2 , D_2 .

Step two: ‘the fused approximation and wavelet coefficients A_c , H_c , V_c and D_c can be obtained after comparison of four sets of coefficients of two images, respectively, according to formula (13):

$$s = \begin{cases} s_1, & s_1 \geq s_2 \\ s_2, & s_1 < s_2 \end{cases} \quad (13)$$

In this formula, s_1 and s_2 represent the approximation and wavelet coefficients A_1 , A_2 , H_1 , H_2 , V_1 , V_2 , D_1 and D_2 . s represents the fused approximation and wavelet coefficients A_c , H_c , V_c and D_c .

Step three: ‘a fused image can be obtained after inverse wavelet transform of the fused approximation and wavelet coefficients A_c , H_c , V_c and D_c .

3.4.2 Intuitionistic fuzzy inference fusion algorithm: Fuzzy inference is a kind of technology which belongs to the category of artificial intelligence. It is a method of inference by imitating human thinking and it realizes the mapping between input and output. Canada's *A Nejatali* and *IR Ceric* first applied fuzzy inference to image fusion theory in 1998 [25]. With the development of research in past twenty years, there have been a small number of fusion algorithms based on intuitionistic fuzzy inference system [26, 27].

The step of intuitionistic fuzzy inference fusion algorithm is as follows:

Step one: ‘registration of input image CT and MRI.

Step two: ‘CT image is decomposed into approximation coefficient A_1 and three wavelet coefficients H_1 , V_1 , D_1 and MRI image is decomposed into approximation coefficient A_2 and three wavelet coefficients H_2 , V_2 , D_2 after wavelet transform.

Step three: ‘fused approximation and wavelet coefficients A_i , H_i , V_i and D_i can be obtained by intuitionistic fuzzy inference method, respectively.

Step four: ‘fused image can be obtained after inverse wavelet transform of fused approximation coefficient and three wavelet coefficients A_i , H_i , V_i and D_i .

In step three, intuitionistic fuzzy inference method refers to Mamdani type intuitionistic fuzzy inference which is proposed by Qi Sun [28].

4 Experimental results and discussion

4.1 Refined weight maps obtained

According to the method discussed in part 3.1, refined weight maps are obtained for fifteen groups of testing images. The values of r and ϵ are automatically obtained by the method in the part 2.2, and different group of images may have different values. Comparisons of W_1 and W_2 with M_1 and M_2 in each group show that the image noise is reduced and the edges are distinct after filtering.

4.2 Experimental results

Figs. 8–15 show the fused images obtained by fifteen groups of testing images from group one to group fifteen.

The evaluation parameters results are listed in Table 1. In Table 1, Choose-m represents Choose-max algorithm, Fuzzy

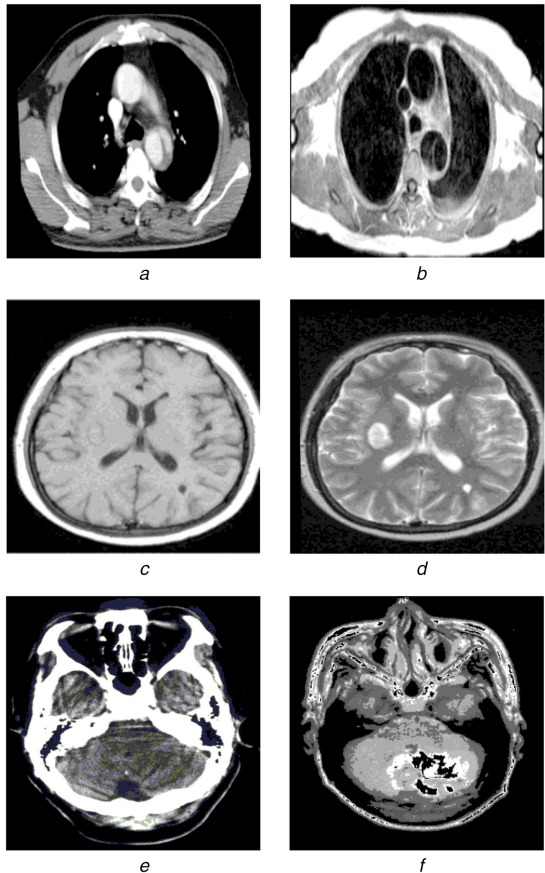


Fig. 5 Testing images of group seven, group eight and group nine
 (a) CT image of group seven, (b) MRI image of group seven, (c) CT image of group eight, (d) MRI image of group eight, (e) CT image of group nine, (f) MRI image of group nine

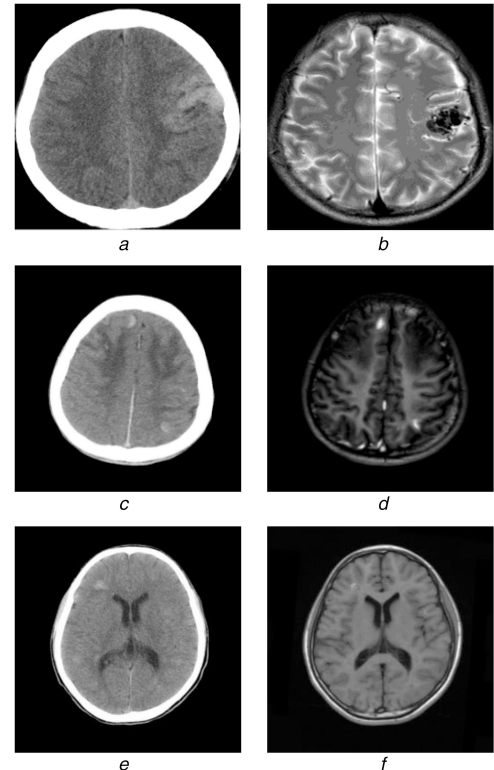


Fig. 7 Testing images of group 13, group 14 and group 15
 (a) CT image of group 13, (b) MRI image of group 13, (c) CT image of group 14, (d) MRI image of group 14 (e) CT image of group 15, (f) MRI image of group 15

represents Intuitionistic fuzzy inference algorithm, proposed represents proposed algorithm.

4.3 Discussion

Figs. 8–15 show the fused images obtained and the evaluation parameters results are listed in Table 1. In Table 1, Choose-m represents Choose-max algorithm, Fuzzy represents Intuitionistic fuzzy inference algorithm, proposed represents proposed algorithm.

For group one:

According to Fig. 8, image (c) is the most clear, and strong sense of hierarchy than image (a) and image (b). According to Table 1, the standard deviation, average gradient and edge strength of proposed algorithm are 0.396315, 0.565875 and 0.129778, respectively. Parameters are obtained at $r=8$. Three evaluation parameters are obviously larger than those of the other two medical images fusion algorithms based on Choose-max fusion algorithm and Intuitionistic fuzzy inference fusion algorithm. It means that the image obtained by proposed algorithm contains the largest amount of information and has better quality.

For group two:

According to Fig. 8, image (d) and image (e) decrease the brightness of the soft tissue and make some details invisible. Image (f) preserves the complementary and detailed information of source images. According to Table 1, the standard deviation, average gradient and edge strength of proposed algorithm are 0.150644, 0.248909 and 0.043825, respectively. Parameters are obtained at $r=53$. Three evaluation parameters are obviously larger than those of the other two medical images fusion algorithms based on Choose-max fusion algorithm and Intuitionistic fuzzy inference fusion algorithm. It means that the image obtained by proposed algorithm contains the largest amount of information and has better quality.

For group three:

According to Fig. 9, image (c) is able to see more clearly the white spots in the human brain. According to Table 1, the standard deviation, average gradient and edge strength of proposed algorithm are 0.190642, 0.316877 and 0.056107, respectively. Parameters are obtained at $r=5$. Three evaluation parameters are

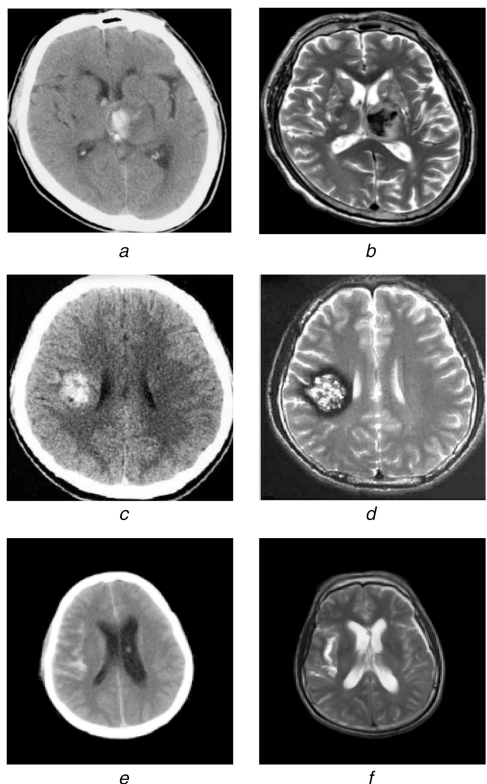


Fig. 6 Testing images of group ten, group 11 and group 12
 (a) CT image of group ten, (b) MRI image of group ten, (c) CT image of group 11, (d) MRI image of group 11, (e) CT image of group 12, (f) MRI image of group 12

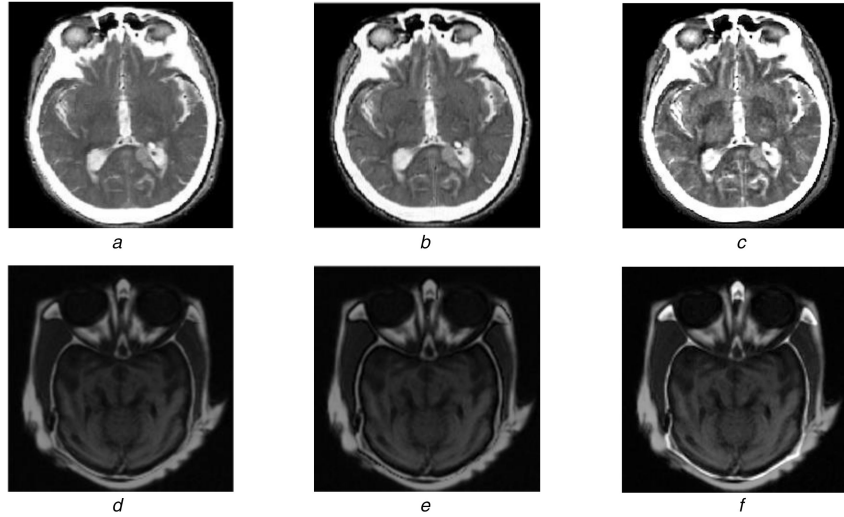


Fig. 8 Fused images of group one and group two **(a)** Fused image of group one by Choose-max fusion algorithm, **(b)** Fused image of group one by Intuitionistic fuzzy inference fusion algorithm, **(c)** Fused image of group one by proposed algorithm, **(d)** Fused image of group two by Choose-max fusion algorithm, **(e)** Fused image of group two by Intuitionistic fuzzy inference fusion algorithm, **(f)** Fused image of group two by proposed algorithm

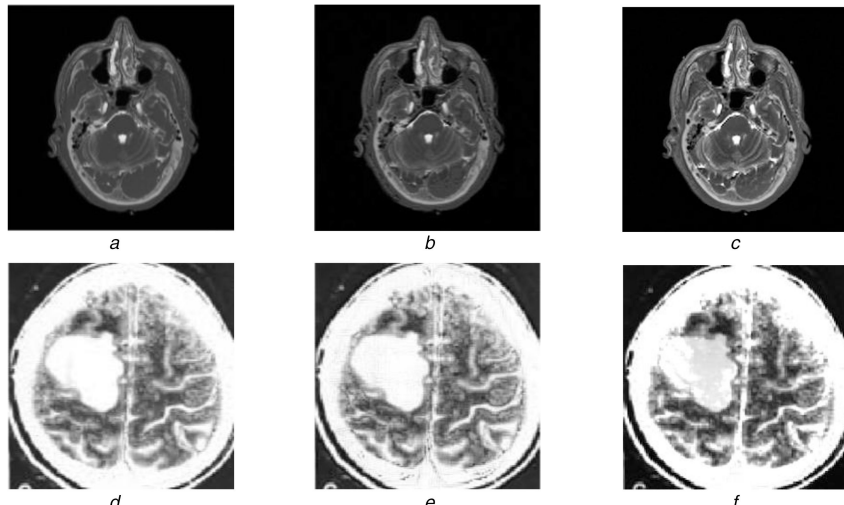


Fig. 9 Fused images of group three and group four **(a)** Fused image of group three by Choose-max fusion algorithm, **(b)** Fused image of group three by Intuitionistic fuzzy inference fusion algorithm, **(c)** Fused image of group three by proposed algorithm, **(d)** Fused image of group four by Choose-max fusion algorithm, **(e)** Fused image of group four by Intuitionistic fuzzy inference fusion algorithm, **(f)** Fused image of group four by Proposed algorithm

obviously larger than those of the other two medical images fusion algorithms based on Choose-max fusion algorithm and Intuitionistic fuzzy inference fusion algorithm. It means that the image obtained by proposed algorithm contains the largest amount of information and has better quality.

For group four:

According to Fig. 9, there is a tumour in the brain, image (f) shows the hierarchy of the tumour more clearly. According to Table 1, the standard deviation, average gradient and edge strength of proposed algorithm are 0.467294, 0.505129 and 0.149525, respectively. Parameters are obtained at $r=52$. Three evaluation parameters are obviously larger than those of the other two medical images fusion algorithms based on Choose-max fusion algorithm

and Intuitionistic fuzzy inference fusion algorithm. It means that the image obtained by proposed algorithm contains the largest amount of information and has better quality.

For group five:

According to Fig. 10, image (c) is the most clear, and strong sense of hierarchy than image (a) and image (b). According to Table 1, the standard deviation, average gradient and edge strength of proposed algorithm are 0.405546, 0.293708 and 0.095406, respectively. Parameters are obtained at $r=95$. Three evaluation parameters are obviously larger than those of the other two medical images fusion algorithms based on Choose-max fusion algorithm and Intuitionistic fuzzy inference fusion algorithm. It means that

$$\begin{aligned} S_x(i, j) &= B_{i-1, j+1} + 2B_{i, j+1} + B_{i+1, j+1} - B_{i-1, j-1} - 2B_{i, j-1} - B_{i+1, j-1} \\ S_y(i, j) &= B_{i+1, j-1} + 2B_{i+1, j} + B_{i+1, j+1} - B_{i-1, j-1} - 2B_{i-1, j} - B_{i-1, j+1} \end{aligned} \quad (10)$$

$$\begin{aligned} \text{HOE}(i, j) &= |B_{i-1, j+1} + 2B_{i, j+1} + B_{i+1, j+1} - B_{i-1, j-1} - 2B_{i, j-1} - B_{i+1, j-1}|/4 \\ \text{VOE}(i, j) &= |B_{i+1, j-1} + 2B_{i+1, j} + B_{i+1, j+1} - B_{i-1, j-1} - 2B_{i-1, j} - B_{i-1, j+1}|/4 \\ \text{DOE}(i, j) &= |2B_{i-1, j-1} + B_{i-1, j} + B_{i, j-1} - 2B_{i+1, j+1} - B_{i, j+1} - B_{i+1, j}|/4 \\ \text{NOE}(i, j) &= |2B_{i-1, j+1} + B_{i-1, j} + B_{i, j+1} - 2B_{i+1, j-1} - B_{i, j-1} - B_{i+1, j}|/4 \end{aligned} \quad (11)$$

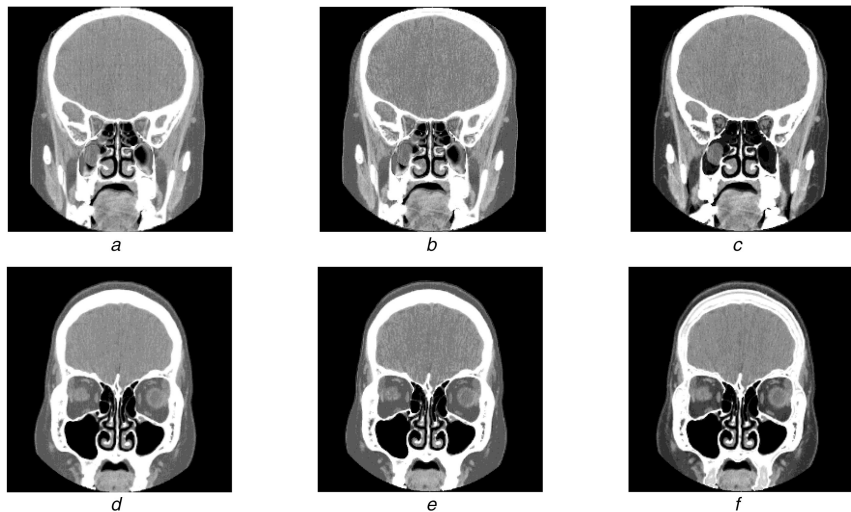


Fig. 10 Fused images of group five and group six (a) Fused image of group five by Choose-max fusion algorithm, (b) Fused image of group five by Intuitionistic fuzzy inference fusion algorithm, (c) Fused image of group five by proposed algorithm, (d) Fused image of group six by Choose-max fusion algorithm, (e) Fused image of group six by Intuitionistic fuzzy inference fusion algorithm, (f) Fused image of group six by proposed algorithm

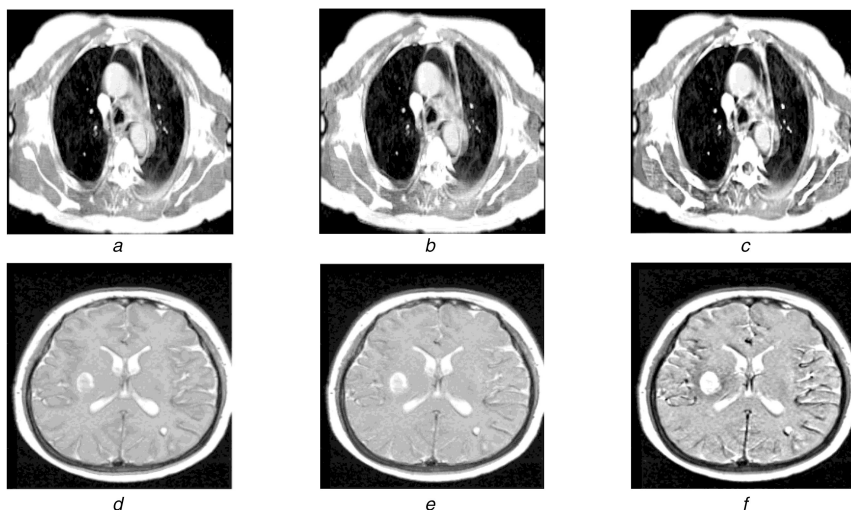


Fig. 11 Fused images of group seven and group eight (a) Fused image of group seven by Choose-max fusion algorithm, (b) Fused image of group seven by Intuitionistic fuzzy inference fusion algorithm, (c) Fused image of group seven by proposed algorithm, (d) Fused image of group eight by Choose-max fusion algorithm, (e) Fused image of group eight by Intuitionistic fuzzy inference fusion algorithm, (f) Fused image of group eight by proposed algorithm

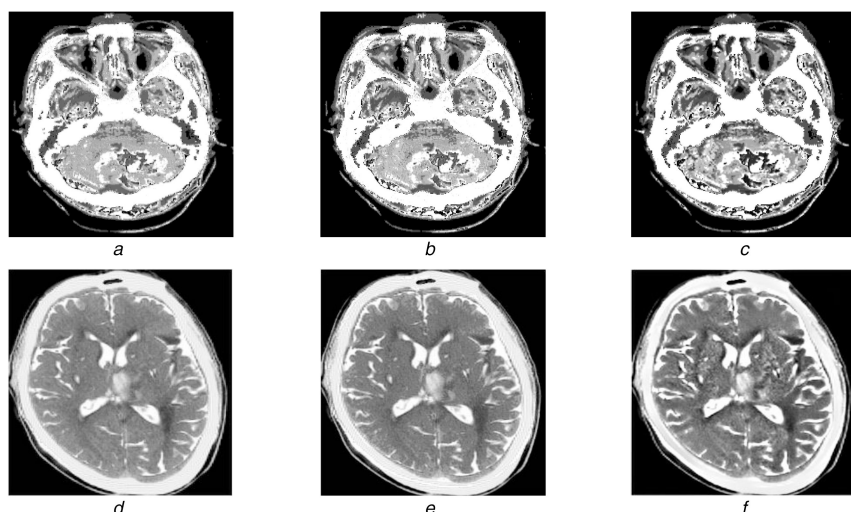


Fig. 12 Fused images of group nine and group ten
(a) Fused image of group nine by Choose-max fusion algorithm, (b) Fused image of group nine by Intuitionistic fuzzy inference fusion algorithm, (c) Fused image of group nine by proposed algorithm, (d) Fused image of group ten by Choose-max fusion algorithm, (e) Fused image of group ten by Intuitionistic fuzzy inference fusion algorithm, (f) Fused image of group ten by proposed algorithm

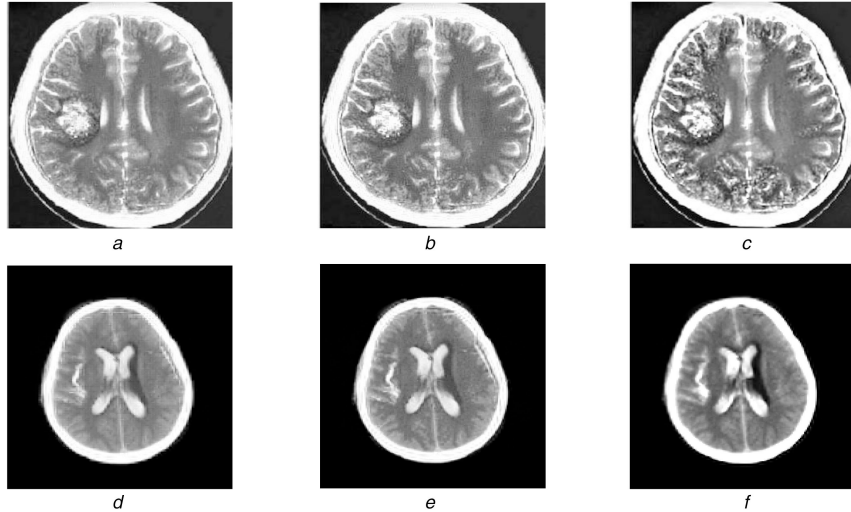


Fig. 13 Fused images of group 11 and group 12 **(a)** Fused image of group 11 by Choose-max fusion algorithm, **(b)** Fused image of group 11 by Intuitionistic fuzzy inference fusion algorithm, **(c)** Fused image of group 11 by proposed algorithm, **(d)** Fused image of group 12 by Choose-max fusion algorithm, **(e)** Fused image of group 12 by Intuitionistic fuzzy inference fusion algorithm, **(f)** Fused image of group 12 by proposed algorithm

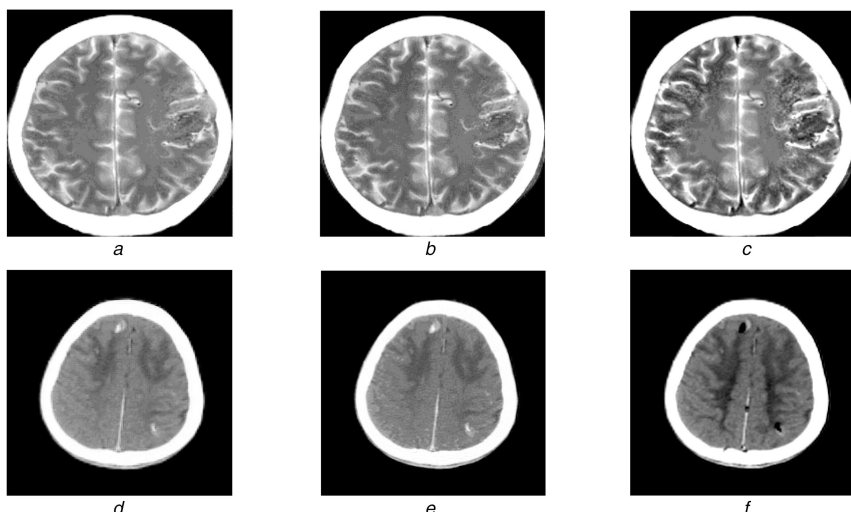


Fig. 14 Fused images of group 13 and group 14 **(a)** Fused image of group 13 by Choose-max fusion algorithm, **(b)** Fused image of group 13 by Intuitionistic fuzzy inference fusion algorithm, **(c)** Fused image of group 13 by proposed algorithm, **(d)** Fused image of group 14 by Choose-max fusion algorithm, **(e)** Fused image of group 14 by Intuitionistic fuzzy inference fusion algorithm, **(f)** Fused image of group 14 by proposed algorithm

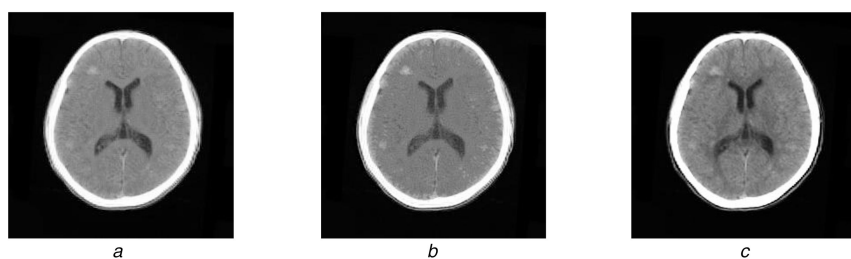


Fig. 15 Fused images of group 15 **(a)** Fused image of group 15 by Choose-max fusion algorithm, **(b)** Fused image of group 15 by Intuitionistic fuzzy inference fusion algorithm, **(c)** Fused image of group 15 by proposed algorithm

the image obtained by proposed algorithm contains the largest amount of information and has better quality.

For group six:

According to Fig. 10, image (f) is the most clear, and strong sense of hierarchy than image (d) and image (e). According to Table 1, the standard deviation, average gradient and edge strength of proposed algorithm are 0.378519, 0.286691 and 0.085695, respectively. Parameters are obtained at $r=95$. Three evaluation parameters are obviously larger than those of the other two medical images fusion algorithms based on Choose-max fusion algorithm and Intuitionistic fuzzy inference fusion algorithm. It means that

the image obtained by proposed algorithm contains the largest amount of information and has better quality.

For group seven:

According to Fig. 11, it is clear that image (c) is more clear to display the circular structure in the middle of fusion image. According to Table 1, the standard deviation, average gradient and edge strength of proposed algorithm are 0.401912, 0.422891 and 0.127223, respectively. Parameters are obtained at $r=4$. Three evaluation parameters are obviously larger than those of the other two medical images fusion algorithms based on Choose-max fusion algorithm and Intuitionistic fuzzy inference fusion

algorithm. It means that the image obtained by proposed algorithm contains the largest amount of information and has better quality.

For group eight:

According to Fig. 11, image (f) is the most clear, and strong sense of hierarchy than image (d) and image (e). According to Table 1, the standard deviation, average gradient and edge strength of proposed algorithm are 0.357443, 0.327215 and 0.103287, respectively. Parameters are obtained at $r=23$. Three evaluation parameters are obviously larger than those of the other two medical images fusion algorithms based on Choose-max fusion algorithm and Intuitionistic fuzzy inference fusion algorithm. It means that the image obtained by proposed algorithm contains the largest amount of information and has better quality.

For group nine:

Table 1 Evaluation parameters of fused images based on different fusion algorithms

Group	Algorithm	Standard deviation	Average gradient	Edge strength
1	choose-m	0.334480	0.484896	0.088775
	fuzzy	0.339249	0.551160	0.106562
	proposed	0.396315	0.565975	0.129778
2	choose-m	0.128983	0.188799	0.037942
	fuzzy	0.129394	0.206837	0.041739
	proposed	0.150644	0.248909	0.043825
3	choose-m	0.173673	0.230504	0.039047
	fuzzy	0.172263	0.261258	0.046388
	proposed	0.190642	0.316877	0.056107
4	choose-m	0.300353	0.421955	0.094221
	fuzzy	0.308577	0.476174	0.117548
	proposed	0.467294	0.505129	0.149525
5	choose-m	0.333399	0.242764	0.066118
	fuzzy	0.344353	0.272878	0.079920
	proposed	0.405546	0.293708	0.095406
6	choose-m	0.340087	0.253344	0.056192
	fuzzy	0.356214	0.279261	0.066722
	proposed	0.378519	0.286691	0.085695
7	choose-m	0.369384	0.366812	0.096935
	fuzzy	0.380704	0.392707	0.104161
	proposed	0.401912	0.422891	0.127223
8	choose-m	0.319005	0.270858	0.067587
	fuzzy	0.331322	0.297149	0.074384
	proposed	0.357443	0.327215	0.103287
9	choose-m	0.402858	0.444855	0.127526
	fuzzy	0.420193	0.526689	0.150470
	proposed	0.449850	0.562874	0.176006
10	choose-m	0.320041	0.507036	0.107444
	fuzzy	0.329655	0.560963	0.120179
	proposed	0.376243	0.593020	0.161540
11	choose-m	0.295324	0.386417	0.094632
	fuzzy	0.310257	0.431321	0.110946
	proposed	0.346690	0.525916	0.150285
12	choose-m	0.329821	0.608395	0.060127
	fuzzy	0.329026	0.650835	0.065586
	proposed	0.368846	0.708023	0.083689
13	choose-m	0.336314	0.310237	0.067666
	fuzzy	0.344773	0.345422	0.074315
	proposed	0.372394	0.379109	0.099187
14	choose-m	0.334927	0.384021	0.043673
	fuzzy	0.332097	0.408051	0.045854
	proposed	0.430053	0.447495	0.068097
15	choose-m	0.288323	0.279285	0.042312
	fuzzy	0.285390	0.304840	0.047024
	proposed	0.356291	0.353127	0.064975

According to Fig. 12, There is a blood clot in the bottom of the fusion image. It is easier to estimate the size of the clot by using the image (c). According to Table 1, the standard deviation, average gradient and edge strength of proposed algorithm are 0.449850, 0.562874 and 0.176006, respectively. Parameters are obtained at $r=5$. Three evaluation parameters are obviously larger than those of the other two medical images fusion algorithms based on Choose-max fusion algorithm and Intuitionistic fuzzy inference fusion algorithm. It means that the image obtained by proposed algorithm contains the largest amount of information and has better quality.

For group ten:

According to Fig. 12, image (f) is the most clear, and strong sense of hierarchy than image (d) and image (e). According to Table 1, the standard deviation, average gradient and edge strength of proposed algorithm are 0.376243, 0.593020 and 0.161540, respectively. Parameters are obtained at $r=5$. Three evaluation parameters are obviously larger than those of the other two medical images fusion algorithms based on Choose-max fusion algorithm and Intuitionistic fuzzy inference fusion algorithm. It means that the image obtained by proposed algorithm contains the largest amount of information and has better quality.

For group eleven:

According to Fig. 13, There is a lesion area in the left of the fusion image. It is easier to estimate the size of the area by using the image (c). According to Table 1, the standard deviation, average gradient and edge strength of proposed algorithm are 0.346690, 0.525916 and 0.150285, respectively. Parameters are obtained at $r=4$. Three evaluation parameters are obviously larger than those of the other two medical images fusion algorithms based on Choose-max fusion algorithm and Intuitionistic fuzzy inference fusion algorithm. It means that the image obtained by proposed algorithm contains the largest amount of information and has better quality.

For group twelve:

According to Fig. 13, image (f) is the most clear, and strong sense of hierarchy than image (d) and image (e). According to Table 1, the standard deviation, average gradient and edge strength of proposed algorithm are 0.368846, 0.708023 and 0.083689, respectively. Parameters are obtained at $r=11$. Three evaluation parameters are obviously larger than those of the other two medical images fusion algorithms based on Choose-max fusion algorithm and Intuitionistic fuzzy inference fusion algorithm. It means that the image obtained by proposed algorithm contains the largest amount of information and has better quality.

For group thirteen:

According to Fig. 14, There is a lesion area in the right of the fusion image. It is easier to estimate the size of the area by using the image (c). According to Table 1, the standard deviation, average gradient and edge strength of proposed algorithm are 0.372394, 0.379109 and 0.099187, respectively. Parameters are obtained at $r=8$. Three evaluation parameters are obviously larger than those of the other two medical images fusion algorithms based on Choose-max fusion algorithm and Intuitionistic fuzzy inference fusion algorithm. It means that the image obtained by proposed algorithm contains the largest amount of information and has better quality.

For group fourteen:

According to Fig. 14, image (f) is the most clear, and strong sense of hierarchy than image (d) and image (e). According to Table 1, the standard deviation, average gradient and edge strength of proposed algorithm are 0.430053, 0.447495 and 0.068097, respectively. Parameters are obtained at $r=57$. Three evaluation parameters are obviously larger than those of the other two medical images fusion algorithms based on Choose-max fusion algorithm and Intuitionistic fuzzy inference fusion algorithm. It means that the image obtained by proposed algorithm contains the largest amount of information and has better quality.

For group fifteen:

According to Fig. 15, image (c) is the most clear, and strong sense of hierarchy than image (b) and image (a). According to Table 1, the standard deviation, average gradient and edge strength of proposed algorithm are 0.356291, 0.353127 and 0.064975,

respectively. Parameters are obtained at $r=65$. Three evaluation parameters are obviously larger than those of the other two medical images fusion algorithms based on Choose-max fusion algorithm and Intuitionistic fuzzy inference fusion algorithm. It means that the image obtained by proposed algorithm contains the largest amount of information and has better quality.

In summary, comparison and analysis of 15 groups experiment date demonstrate that the marginalisation degree, image definition and tiny detail contrast of the fused images based on proposed algorithm are the best one. So the proposed fusion algorithm is better than Choose-max fusion algorithm and Intuitionistic fuzzy inference fusion algorithm.

4.4 Medical evaluation

Comparing the results of the three fusion algorithms, we can see that the fused image obtained by proposed algorithm is more clear, and better preserves the details of CT and MRI images.

The fused images contain more abundant, visual and comprehensive information, acquiring new diagnosis information, and will be helpful for precisely identifying lesion' Spatial location, size, geometrical shape and increasing the accuracy of disease diagnosis.

By using the fused images, experienced radiotherapist can acquire higher accuracy clinical diagnosis for the tumour target volume and will benefit for patient precision targeted therapy.

The malignant tumour postoperative target identified by radiotherapist by using the fused image will be smaller than CT positioning imaging, and will reduce the volume normal tissue exposed to radiation source and improve the target volume dosage, narrow the diagnosis discrepancies between different physicians and better protect the patients.

5 Conclusion

The design of weight coefficients is the key of weighted fusion algorithm in transform domain. The feature of this paper is that a GF is designed with the weight map serving as input image and the corresponding approximation coefficient serving as guided image. The GF is used to process the weight map to obtain the refined weight map. Thus the refined weight map of each image is different and determined by the characteristics of the image to be fused. So, the algorithm proposed in this paper can fuse images adaptively.

In this algorithm, approximation coefficient and three wavelet coefficients of CT and MRI are obtained by using a wavelet transform on CT and MRI medical images, respectively. The weight maps are obtained by comparing the two approximation coefficients pixel by pixel. The refined weight maps are obtained by using the GF to smooth the weight maps. The approximation and wavelet coefficients of CT and MRI images are fused together by using the refined weight maps. A fused image of CT and MRI is obtained by the inverse wavelet transform.

Comparing the results of the three fusion algorithms, we can see that the fused image obtained by the algorithm proposed is more clear, and better preserves the details of CT and MRI images. Therefore, this algorithm is more advantageous than the other two algorithms to locate the position and shape of the target volume, and improve the target volume delineation efficiency. In the course of treatment, can better avoid the surrounding health organs by radiation, protect the health of patients.

Further research on images fusion algorithm can be done by combination of GF with multi-layer and multi-scale transform.

6 Acknowledgments

This research work is supported by the National Natural Science Foundation of China under Grant No. 61271298. CT and MRI

images used in experiments are down loaded from network; many thanks go to the providers.

7 References

- [1] Zhao, Y., Zhao, Q., Hao, A.: 'Multimodal medical image fusion using improved multi-channel PCNN', *Biomed. Mater. Eng.*, 2014, **24**, pp. 221–228
- [2] Chen, L., Pan, J., Chen, C.: 'Clinical research of target contour in NPC IMRT using CT/MRI fusion technique', *Int. Med. Health Guid. News*, 2008, **14**, (1), pp. 4–7
- [3] Wang, L., Tao, L., Wang, H.: 'The research on evaluate measure of CT and MRI image fusion', *J. Biomed. Eng. Res.*, 2006, **25**, (4), pp. 247–250
- [4] Lizhen, C.A.O., Li, K., Zhao, X.: 'The diagnostic application of registration of CT and MR images in craniocerebral tumour', *J. Clin. Radiol.*, 2004, **23**, (12), pp. 1023–1026
- [5] Xing, Z., Lin, Z.: 'Fusion of PET images with CT and MR images in diagnosing tumours', *Chin. J. CT MRI*, 2005, **25**, (5), p. 290
- [6] Wenqi, D., Yunfeng, Z., Yahua, Z.: 'Application of CT and MRI image fusion in radiotherapy of head and neck tumours', *Chin. J. Radiat. Oncol. Biol.*, 2007, **16**, (5), pp. 397–398
- [7] Rong, H., Hui, W., Xiaoxu, L.: 'Observation of CT-MRI image fusion in postoperativeprecise radiotherapy for gliomas', *Chin. J. Radiat. Oncol. Biol.*, 2017, **26**, (2), pp. 192–196
- [8] Gan, X., Xu, Z., Liao, F.: 'Application value of CT/MRI image fusion technique in the delineating of target area for radiotherapy of nasal pharyngeal cancer', *China Med. Dev.*, 2014, **29**, (11), pp. 163–165
- [9] Xu, Q., Zhou, Y., Wang, W., et al.: 'An algorithm of remote sensing image fusion based on nonsubsampled contourlet transform', 2012 5th Int. Congress on Image and Signal Processing, Chongqing, China, 2012, pp. 1005–1009
- [10] Zhu, J., Che, J., Guo, Z.: 'Curvete algorithm of the remote sensing image fusion based on the local mean and standard deviation', *J. Ningxia Univ. (Nat. Sci. Ed.)*, 2014, **35**, (1), pp. 24–27
- [11] Xu, Y.: 'Research and application of image fusion method based on wavelet transform technique'. Master's degree thesis, Shandong Normal University, 2008
- [12] Prakash, C., Rajkumar, S., Mouli, P.C.: 'Medical image fusion based on redundancy DWT and Mamdani type min-sum mean-of-max techniques with quantitative analysis', Proc. Int. Conf. Recent Advances in Computing and Software Systems, Piscataway, NJ, 2012, pp. 54–59
- [13] Tomasi, Y., Manduchi, R.: 'Bilateral filtering for gray and color images'. IEEE Int. Conf. Computer Vision, Piscataway, NJ, 1998, pp. 839–846
- [14] Petschnigg, G., Agrawala, M., Hoppe, H., et al.: 'Digital photography with flash and no-flash image pairs', Proc. of the ACM SIGGRAPH Conf. ACM Transactions on Graphics, New York, NY, 2004, pp. 664–672
- [15] Durand, F., Dorsey, J.: 'Fast bilateral filtering for the display of high dynamic-range images', 'ACM transactions on graphics'. Proc. ACM SIGGRAPH Conf., New York, NY, 2002, pp. 257–266
- [16] He, K., Sun, J., Tang, X.: 'Guided image filtering', *Pattern Anal. Mach. Intell.*, 2012, **35**, pp. 1397–1409
- [17] Fang, S., Yang, J., Cao, Y., et al.: 'Local multi-scale retinex algorithm based on guided image filtering', *J. Image Graph.*, 2012, **17**, (7), pp. 748–755
- [18] Liu, N., Zhao, D.: 'Detail enhancement for high-dynamic-range infrared images based on guided image filter', *Infrared Phys. Technol.*, 2014, **67**, pp. 138–147
- [19] Lin, Z., Wang, X.: 'Dehazing for image and video using guided filter', 2012 World Congress on Engineering and Technology, Beijing, China, 2012, pp. 123–127
- [20] Li, S., Kang, X., Hu, J.: 'Image fusion with guided filtering', *IEEE Trans. Image Process.*, 2013, **22**, (7), pp. 2864–2875
- [21] Mehra, I., Naveen, K.N.: 'Image fusion using wavelet transform and its application to asymmetric cryptosystem and hiding', *Opt. Soc. Am.*, 2014, **22**, pp. 5474–5482
- [22] Xue, X., Peng, J., Yuan, C.: 'An efficient fusion algorithm of panchromatic and multi-Spectral remote sensing images based on wavelet transform'. Int. Conf. Information and Automation, Piscataway, NJ, 2013
- [23] Ren, X.: 'Research and implementation of objective assessment methods of image quality'. Master's degree thesis, Nanjing University of Aeronautics and Astronautics, 2008
- [24] Wu, L.: 'Research of interactive segmentation algorithm of medical image'. Master's degree thesis, Electronic Science and Technology of China, 2008
- [25] Nejatali, A., Ciric, I.R.: 'Novel image fusion methodology using fuzzy set theory', *Opt. Eng.*, 1998, **37**, (2), pp. 485–491
- [26] Zhao, M., Na, Y., Li, S.: 'Research on medical image fusion method based on intuitionistic fuzzy reasoning', *Electron. Technol.*, 2012, **25**, (13), pp. 48–50
- [27] Li, S.: 'Research on medical image fusion algorithm based on intuitionistic fuzzy reasoning'. Master's degree thesis, Xidian University, 2011
- [28] Sun, Q., Na, Y., Liu, B.: 'Image fusion algorithm based on Mamdani intuitionistic fuzzy inference system', *Electron. Sci. Technol.*, 2014, **27**, (5), pp. 193–196